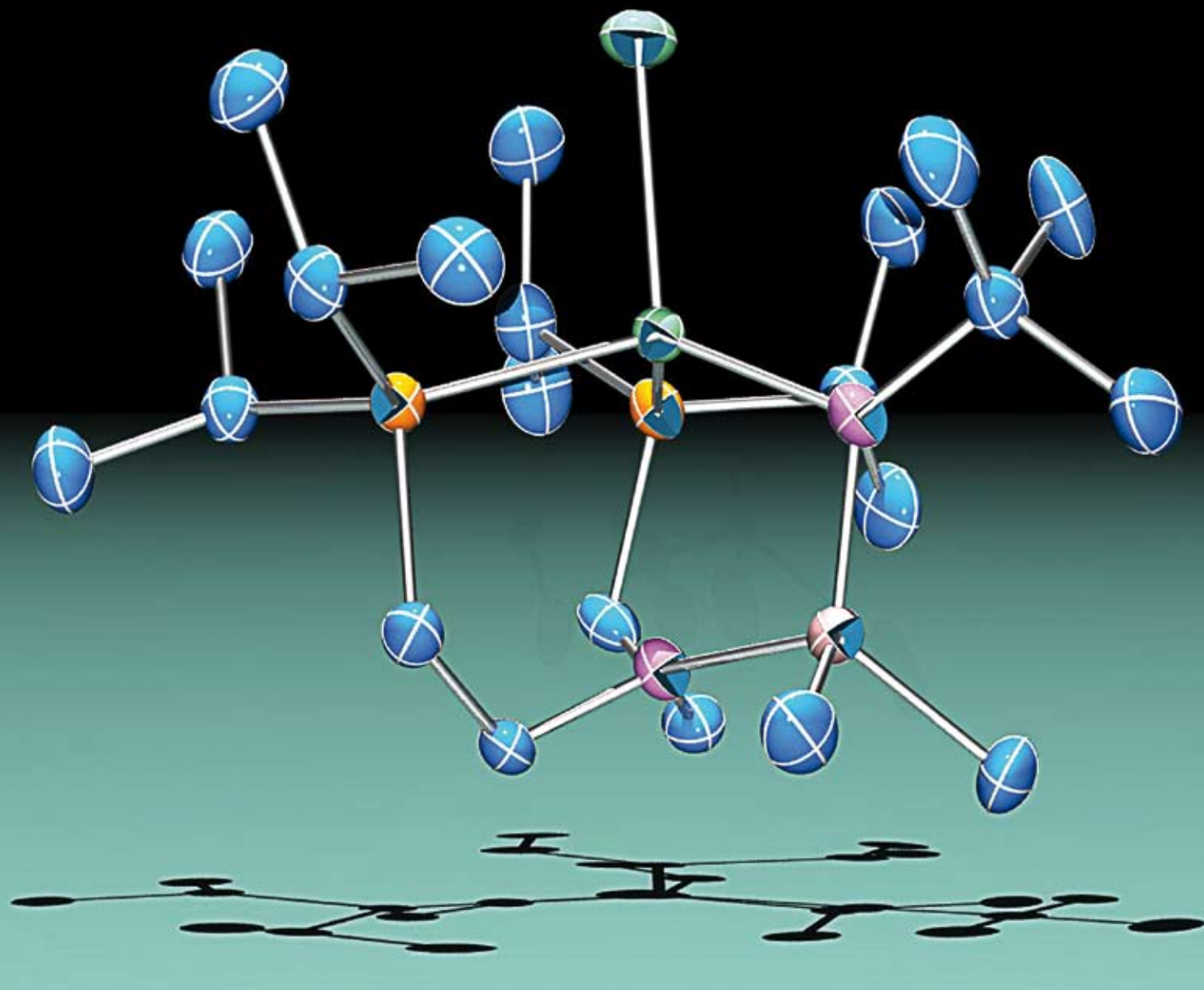


Dalton Transactions

An international journal of inorganic chemistry

www.rsc.org/dalton

Number 10 | 14 March 2009 | Pages 1677–1872



ISSN 1477-9226

RSC Publishing

PAPER

Arnold and Chomitz
Synthesis and characterization of manganese and iron complexes supported by multidentate $[N_2P_2]$ ligands

PAPER

Williams, Záliš *et al.*
Tipping the balance from localised to intraligand charge-transfer excited states in cyclometalated platinum complexes

COMMUNICATION

Guo, Wang *et al.*
Fabrication of water soluble and biocompatible CdSe nanoparticles in apoferritin with the aid of EDTA

Synthesis and characterization of manganese and iron complexes supported by multidentate $[\text{N}_2\text{P}_2]$ ligands†

Wayne A. Chomitz and John Arnold*

Received 8th December 2008, Accepted 9th January 2009

First published as an Advance Article on the web 26th January 2009

DOI: 10.1039/b821954k

The coordination chemistry of mono- and divalent manganese and iron complexes supported by the monoanionic multidentate ligands, $[\text{N}_2\text{P}_2]$ (where $[\text{N}_2\text{P}_2] = \text{tBuN}^-(\text{SiMe}_2\text{N}(\text{CH}_2\text{CH}_2\text{P}^i\text{Pr}_2)_2)$ and $[\text{N}_2\text{P}_2^{\text{tolyl}}]$ (where $[\text{N}_2\text{P}_2^{\text{tolyl}}] = \text{MeC}_6\text{H}_4\text{N}^-(\text{SiMe}_2(\text{CH}_2\text{CH}_2\text{P}^i\text{Pr}_2)_2)$ is presented. The Mn(II) and Fe(II) halide complexes $[\text{N}_2\text{P}_2]\text{MnCl}$ (**1**) and $[\text{N}_2\text{P}_2]\text{FeCl}$ (**2**) serve as precursors to the alkyl and hydride species $[\text{N}_2\text{P}_2]\text{MnMe}$ (**3**), $[\text{N}_2\text{P}_2]\text{FeMe}$ (**4**), $[\text{N}_2\text{P}_2]\text{FeCH}_2\text{SiMe}_3$ (**5**), and $([\text{N}_2\text{P}_2]\text{Mn})_2(\mu\text{-H})_2$ (**6**).

Reduction of **1** and **2** results in the formation of the new bridging dinitrogen complexes $([\text{N}_2\text{P}_2]\text{Mn})_2(\mu\text{-N}_2)$ (**7**) and $([\text{N}_2\text{P}_2]\text{Fe})_2(\mu\text{-N}_2)$ (**8**), respectively. Upon exposure to vacuum, N_2 is abstracted from **8**, resulting in the observed Fe(I) complex, $[\text{N}_2\text{P}_2]\text{Fe}$ (**9**). The new Fe(II) halide complex $[\text{N}_2\text{P}_2^{\text{tolyl}}]\text{FeCl}$ (**10**) was isolated following the substitution of $[\text{N}_2\text{P}_2^{\text{tolyl}}]$ for $[\text{N}_2\text{P}_2]$. Reduction of **10** in the presence of N_2 resulted in the formation of the dinitrogen free adduct $[\text{N}_2\text{P}_2^{\text{tolyl}}]\text{Fe}$ (**11**).

Introduction

First-row middle-transition metal complexes have proven to be useful catalysts for a number of important transformations. Brookhart *et al.*,¹ Gibson *et al.*,² and Bennett³ have reported highly active ethylene polymerization catalysts incorporating bulky bis(imino)pyridine ligands with Fe and Co. By reducing the steric bulk of the bis(imino)pyridine ligand, it was discovered that selective oligomerization of ethylene to linear α -olefins could be achieved.⁴ The utility of bis(imino)pyridine ligands was extended to include Mn by Gambarotta and co-workers who reported multi-electron reduction at the metal center following alkylation.⁵ More recently, Chirik *et al.* reported the synthesis of reduced Fe complexes supported by bis(imino)pyridine ligands and their application for hydrogenation and hydrosilation.⁶ First-row metal-hydride species have also been shown to be active in stoichiometric reactions, as shown by Holland *et al.* who observed azobenzene $\text{N}=\text{N}$ bond cleavage by a three coordinate iron hydride.⁷

The activation and functionalization of N_2 using transition metal complexes is also an important research topic.^{8–13} The industrial standard for N_2 fixation is the Haber–Bosch process, which converts N_2 and H_2 to NH_3 using an ill-defined Fe catalyst.¹⁴ Though extremely good conversion rates (98%) can be achieved, a tremendous amount of energy is consumed (1% of world energy consumption).¹⁵ In contrast, nature uses nitrogenase enzymes to catalytically reduce atmospheric N_2 to ammonium salts, which are then used to synthesize useful nitrogen-containing molecules. Nitrogenase operates under ambient conditions and also contains an Fe catalyst.^{16–19} Given the role low-valent middle transition metals play in the above catalytic reactions, their chemistry with N_2 has become a recent topic of interest.^{6,20–26}

Here we report our findings on the application of $[\text{N}_2\text{P}_2]$ as a supporting ligand for organometallic and low-valent species of Mn and Fe. The synthesis of a number of metal-alkyl, metal-hydride, and low-valent compounds is described, and the reactivity of reduced Mn and Fe complexes of $[\text{N}_2\text{P}_2]$ with N_2 is explored. Finally, the modified $[\text{N}_2\text{P}_2]$ ligand, $[\text{N}_2\text{P}_2^{\text{tolyl}}]$, is introduced into the Fe system and the resulting changes in reactivity with N_2 are examined.

Experimental

All reactions were performed using standard Schlenk-line techniques or in an MBraun drybox (<1 ppm $\text{O}_2/\text{H}_2\text{O}$) unless noted otherwise. All glassware, cannulae, and Celite® were stored in an oven at >425 K. Pentane, toluene, diethyl ether, and tetrahydrofuran were purified by passage through a column of activated alumina and degassed with nitrogen prior to use.²⁷ Deuterated solvent was vacuum transferred from sodium/benzophenone (benzene). NMR spectra were recorded at ambient temperature on Bruker AV-300, AVQ-400, AVB-400, and DRX-500 spectrometers. ^1H and $^{13}\text{C}\{^1\text{H}\}$ chemical shifts are given relative to residual solvent peaks, and coupling constants (J) are given in hertz. $^{31}\text{P}\{^1\text{H}\}$ chemical shifts are referenced to an external standard of $\text{P}(\text{OMe})_3$ set to 1.67 ppm. Infrared samples were prepared as Nujol mulls and taken between KBr disks. Magnetic susceptibility (μ_{eff}) values were determined using the solution Evans method at ambient temperature (22 °C).²⁸ Melting points were determined using sealed capillaries prepared under nitrogen and are uncorrected. $\text{Li}[\text{N}_2\text{P}_2]$,²⁹ $\text{Li}[\text{N}_2\text{P}_2^{\text{tolyl}}]$,³⁰ $[\text{N}_2\text{P}_2]\text{MnCl}$ (**1**),²⁹ and $[\text{N}_2\text{P}_2]\text{FeCl}$ (**2**)²⁹ were prepared using the literature procedures, and unless otherwise noted, all reagents were acquired from commercial sources. Elemental analyses and mass spectral data were determined at the College of Chemistry, University of California, Berkeley. The X-ray structural determination was performed at CHEXRAY, University of California, Berkeley.

Department of Chemistry, University of California, Berkeley, CA 94720-1460, USA. E-mail: arnold@berkeley.edu; Tel: +1 510-643-5381

† CCDC reference numbers 711736 and 711737. For crystallographic data in CIF or other electronic format see DOI: 10.1039/b821954k

[N₂P₂]MnMe (3)

Methyl lithium (1.6 M in Et₂O, 0.36 mL, 0.57 mmol) was syringed into a solution of **1** (0.30 g, 0.57 mmol) in 10 mL Et₂O at -40 °C. The reaction mixture was warmed to room temperature and was stirred for 4 h. The solvent was removed under vacuum, and the crude product was extracted with pentane. Following concentration and cooling at -40 °C, large colorless needles were isolated in 56% yield (0.16 g). ¹H NMR (300 MHz, C₆D₆): δ 0.267 (s); 1.10 (s); 1.67 (s); 3.24 (s); 6.07 (s). IR (cm⁻¹): 1346 (m); 1297 (w); 1245 (m); 1199 (s); 1101 (m); 1056 (s); 1017 (m); 969 (w); 926 (w); 882 (w); 844 (s); 794 (m); 752 (m); 727 (s); 685 (w); 649 (m); 597 (w); 526 (m); 439 (m). Anal. Calc. C₂₃H₃₄MnN₂P₂Si. C: 54.83; H: 10.83; N: 5.56. Observed. C: 54.45; H: 11.08; N: 5.47. mp = 85–86 °C. μ_{eff} = 5.7 μ_B.

[N₂P₂]FeMe (4)

Methyl lithium (1.0 M in Et₂O, 0.60 mL, 0.60 mmol) was added to a solution of **2** (0.30 g, 0.57 mmol) in 7 mL THF at -40 °C *via* syringe. The reaction mixture was allowed to warm to room temperature and was stirred for 3 h. The volatile material was removed under vacuum, and the crude product was extracted with pentane. Following concentration and cooling at -40 °C, large yellow needles were isolated in 54% yield (0.16 g). ¹H NMR (300 MHz, C₆D₆): δ -2.49 (br s); 0.24 (s); 1.10 (s); 1.65 (s); 3.25 (s); 17.61 (br s); 26.85 (br s); 44.90 (br s); 56.55 (br s); 61.10 (br s); 73.40 (br s). IR (cm⁻¹): 1643 (w); 1306 (w); 1243 (s); 1196 (s); 1113 (s); 1050 (s); 1016 (s); 970 (w); 926 (m); 882 (w); 843 (s); 797 (m); 753 (m); 733 (m); 683 (w); 653 (m); 600 (w); 549 (w); 529 (w); 462 (m). Anal. Calc. C₂₃H₃₄FeN₂P₂Si. C: 54.74; H: 10.81; N: 5.55. Observed. C: 54.73; H: 11.01; N: 5.41. mp = 99–101 °C. μ_{eff} = 5.0 μ_B.

[N₂P₂]FeCH₂SiMe₃ (5)

A solution of LiCH₂SiMe₃ (0.056 g, 0.59 mmol) in 5 mL THF was added to a solution of **2** (0.31 g, 0.59 mmol) in 5 mL THF at -40 °C. The reaction mixture was allowed to warm to room temperature and was stirred overnight. Solvent was removed under vacuum, and the crude product was extracted with pentane. Following concentration and cooling at -40 °C, colorless plates were collected in 77% yield (0.26 g). ¹H NMR (300 MHz, C₆D₆): δ -5.42 (br s); -2.46 (br s); 0.24 (s); 1.10 (s); 1.65 (s); 2.07 (br s); 3.21 (s); 4.63 (s); 16.77 (br s); 26.04 (br s). IR (cm⁻¹): 1348 (m); 1292 (w); 1235 (s); 1077 (s); 1055 (s); 1028 (m); 966 (w); 880 (s); 846 (s); 817 (s); 769 (m); 736 (m); 719 (m); 665 (m); 607 (m); 536 (w); 519 (m); 487 (m); 455 (m). Anal. Calc. C₂₆H₆₂FeN₂P₂Si₂. C: 54.13; H: 10.86; N: 4.86. Observed. C: 54.25; H: 11.22; N: 4.68. mp = 70–72 °C. μ_{eff} = 5.1 μ_B.

[N₂P₂]Mn)₂(μ-H)₂ (6)

A solution of Red-Al[®] (70% in toluene, 0.18 g, 0.57 mmol) in 5 mL THF was added to a solution of **1** (0.30 g, 0.57 mmol) in 5 mL THF at -40 °C. The reaction mixture was warmed to room temperature and was stirred for 30 min. Solvent was removed under vacuum, and the crude product was extracted with pentane. Following concentration and cooling at -40 °C, colorless crystals were isolated in 57% yield (0.16 g). ¹H NMR (500 MHz, C₆D₆):

δ 0.24 (s); 0.62 (s); 0.88 (s); 1.08 (s); 1.17 (s); 1.65 (s); 3.23 (s); 8.14 (br s); 16.30 (br s). IR (cm⁻¹): 1790 (w); 1349 (m); 1294 (w); 1238 (m); 1200 (s); 1093 (s); 1066 (s); 938 (m); 908 (m); 879 (w); 836 (s); 824 (m); 795 (m); 760 (s); 722 (m); 689 (w); 665 (w); 610 (w); 564 (m); 527 (w); 502 (m). Anal. Calc. C₄₄H₁₀₄Mn₂N₄P₄Si₂. C: 53.95; H: 10.72; N: 5.72. Observed. C: 53.99; H: 11.01; N: 5.83. mp = 104–106 °C. μ_{eff} = 3.4 μ_B per Mn.

([N₂P₂]Mn)₂(μ-N₂) (7)

A freshly prepared solution of sodium naphthalide (0.57 mmol) in 5 mL THF was added to a suspension of **1** (300 mg, 0.57 mmol) in 5 mL THF at -40 °C. The reaction mixture turned dark red instantly and was allowed to warm to room temperature. After stirring for 2 h, the solvent was removed under vacuum. Naphthalene was removed by sublimation, and the crude product was extracted with pentane (10 mL). The solution was concentrated until the precipitation of crystalline material was observed. Cooling at -40 °C resulting in the isolation of large dark red blocks (69 mg, 24% yield). IR (cm⁻¹): 1298 (w); 1229 (s); 1196 (m); 1111 (m); 1050 (s); 1017 (s); 927 (m); 833 (s); 776 (m); 689 (m); 646 (m); 490 (m). Raman (cm⁻¹): 1685 (ν_{N-N}). Anal. Calc. for C₄₄H₁₀₂N₆P₂Si₂Mn₂. C: 52.56; H: 10.25; N: 8.36. Observed. C: 52.68; H: 10.55; N: 8.31. mp (dec) = 108–111 °C. μ_{eff} = 8.7 μ_B.

([N₂P₂]Fe)₂(μ-N₂) (8)

A suspension of KC₈ (0.36 g, 2.7 mmol) in 10 mL THF was added to a suspension of **2** (1.4 g, 2.7 mmol) in 15 mL THF at -40 °C. The reaction mixture was allowed to warm to room temperature and was stirred for 3 h. The solvent was removed under vacuum, and the crude product was extracted with pentane. Following concentration and cooling at -40 °C, large dark red block were isolated (1.1 g, 80% yield). IR (cm⁻¹): 1417 (w); 1349 (m); 1300 (w); 1239 (m); 1201 (m); 1105 (m); 1077 (w); 1047 (s); 1015 (m); 921 (s); 885 (m); 839 (s); 802 (w); 730 (s); 689 (w); 652 (w); 603 (w); 511 (w); 487 (s). Raman (cm⁻¹): 1760 (ν_{N-N}). Anal. Calc. for C₄₄H₁₀₂N₆P₄Si₂Fe₂. C: 52.46; H: 10.23; N: 8.35. Observed. C: 52.74; H: 10.50; N: 7.97. mp = 115–116 °C. μ_{eff} = 7.0 μ_B.

[N₂P₂]Fe (9)

Method A. A dark red solution of **8** (0.30 g, 0.30 mmol) in 10 mL pentane was exposed to vacuum until dryness. Over the course of the solvent evacuation, the solution changed color from dark red to yellow-green. The resulting solid was identified as [N₂P₂]Fe based on the absence of any distinguishing features in the IR spectrum between 1600 and 2700 cm⁻¹ and the isolation of **8** upon exposure of **9** to an atmosphere of N₂. The green color remained as long as negative pressure or an Ar atmosphere was maintained.

Method B. An Ar atmosphere was used instead of N₂, and all solvents were degassed with Ar prior to use. A suspension of KC₈ (77 mg, 0.57 mmol) in 5 mL THF was added to a suspension of **2** (0.30 g, 0.57 mmol) in 5 mL THF at -40 °C. The reaction mixture was allowed to warm to room temperature and was stirred overnight. The reduction of **2** was slower in the absence of N₂, so longer reaction times were needed for the reaction to go to completion. The volatile materials were

Table 1 Crystal data and structure refinement for **5–8**

Compound number	5	6	7	8
Compound name	[N ₂ P ₂]FeCH ₂ SiMe ₃	([N ₂ P ₂]Mn) ₂ (μ-H) ₂	([N ₂ P ₂]Mn) ₂ (μ-N ₂)	([N ₂ P ₂]Fe) ₂ (μ-N ₂)
Empirical formula	C ₂₆ H ₆₂ FeN ₂ P ₂ Si ₂	C ₂₂ H ₅₂ MnN ₂ P ₂ Si	C ₂₂ H ₅₁ MnN ₃ P ₂ Si	C ₂₂ H ₅₁ FeN ₃ P ₂ Si
FW	576.75	979.25	502.63	503.54
Temperature/K	160(2)	160(2)	151(2)	154(2)
Crystal system	Triclinic	Monoclinic	Orthorhombic	Monoclinic
Space group	<i>P</i> $\bar{1}$	<i>C</i> 2/ <i>c</i>	<i>Pbca</i>	<i>P</i> 2 ₁ / <i>c</i>
<i>a</i> /Å	8.6908(11)	49.385(5)	18.381(2)	11.648(1)
<i>b</i> /Å	9.9321(13)	10.9384(11)	15.461(2)	18.056(2)
<i>c</i> /Å	21.345(3)	22.807(2)	19.772(2)	13.382(1)
α /°	96.779(2)	90	90	90
β /°	97.816(2)	107.880(3)	90	102.055(1)
γ /°	104.621(2)	90	90	90
<i>V</i> /Å ³	1743.8(4)	11725(2)	5619.0(11)	2752.3(5)
<i>Z</i>	2	8	8	4
λ /Å	0.71073	0.71073	0.71073	0.71073
μ /cm ⁻¹	0.609	0.611	0.64	0.72
Number of reflections _{obs}	4920	7019	4787	5248
<i>R</i> _(int)	0.0260	0.0722	0.1055	0.0162
<i>R</i> _{obs} (%)	4.86	4.79	5.34	3.19
<i>wR</i> _{obs} (%)	11.85	9.96	12.63	8.83

removed under vacuum, and the crude product was extracted with Et₂O. Following concentration and cooling at –40 °C, yellow-green crystals of **9** were obtained. The yield was not obtained directly due to conversion of **9** to **8** following exposure to N₂.

[N₂P₂^{tolyl}]FeCl (**10**)

A solution of Li[N₂P₂^{tolyl}] (1.0 g, 2.1 mmol) in 20 mL was added dropwise to a suspension of FeCl₂ (0.27 g, 2.1 mmol) in 20 mL DME. The reaction mixture was stirred overnight. The solvent was removed under vacuum, and the crude product was dissolved in THF and filtered through a bed of Celite®. An equal volume of pentane was added, and the resulting solution was cooled at –40 °C overnight. Bright orange crystals were isolated in 70% yield (0.82 g). ¹H NMR (500 MHz, C₆D₆): δ –70.29 (br s); 1.03 (br s); 9.40 (br s); 13.87 (br s); 29.75 (br s); 33.62 (br s); 40.07 (s); 57.78 (br s); 61.22 (br s); 68.28 (s); 72.86 (br s); 87.59 (br s). IR (cm⁻¹): 1606 (s); 1503 (s); 1306 (w); 1265 (s); 1239 (m); 1178 (w); 1118 (m); 1095 (m); 1067 (m); 1049 (m); 997 (w); 973 (w); 930 (s); 887 (w); 844 (s); 800 (m); 762 (s); 682 (m); 663 (m); 601 (m); 547 (w); 506 (m); 456 (w). Anal. Calc. C₂₅H₄₀ClFeN₂P₂Si. C: 53.70; H: 8.85; N: 5.01. Observed. C: 53.49; H: 9.02; N: 4.93. mp = 208–209 °C. $\mu_{\text{eff}} = 4.7 \mu_{\text{B}}$.

Crystallographic analysis†

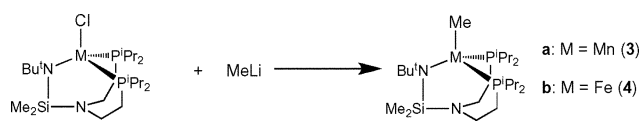
Single crystals of **5–8** were coated in Paratone-N oil, mounted on a Kapton loop, transferred to a Siemens SMART diffractometer or a Bruker APEX CCD area detector,³¹ centered in the beam, and cooled by a nitrogen flow low-temperature apparatus that has been previously calibrated by a thermocouple placed at the same position as the crystal. Preliminary orientation matrices and cell constants were determined by collection of 60 30-second frames, followed by spot integration and least-squares refinement. An arbitrary hemisphere of data was collected and the raw data were integrated using SAINT.³² Cell dimensions reported were calculated from all reflections with *I* > 10 σ . The data were corrected for Lorentz and polarization effects, but no correction

for crystal decay was applied. Data were analyzed for agreement and possible absorption using XPREP.³³ An empirical absorption correction based on comparison of redundant and equivalent reflections was applied using SADABS.³⁴ The structures were solved using SHELXS³⁵ and refined on all data by full-matrix least squares with SHELXL-97.³⁶ Thermal parameters for all non-hydrogen atoms were refined anisotropically. ORTEP diagrams were created using ORTEP-3. A summary of the X-ray diffraction data is presented in Table 1.

Results and discussion

Substitution chemistry of **1** and **2**

The metal-halides [N₂P₂]MnCl (**1**) and [N₂P₂]FeCl (**2**) were synthesized as reported.²⁹ Reaction of **1** and methyl lithium in Et₂O at –40 °C resulted in the isolation of large colorless needles of [N₂P₂]MnMe (**3**) in 56% yield following work-up and crystallization from pentane at –40 °C (Scheme 1a). The solution magnetic susceptibility of **3** is 5.7 μ_{B} (*S* = 5/2), in agreement with high-spin Mn(II). A similar reaction of **2** resulted in large yellow needles of [N₂P₂]FeMe (**4**) in 54% yield (Scheme 1b). The solution magnetic susceptibility of **4** is 5.0 μ_{B} , indicating the presence of high-spin Fe(II). Interestingly, the Co analogue, [N₂P₂]CoMe, is low-spin, and the solid-state structure shows a trigonal bipyramidal geometry about the Co atom.³⁰ No crystallographic data for **3** or **4** could be obtained due to inherent twinning of the crystals. However, based on magnetic data, we infer that the solid-state structures of **3** and **4** are likely tetrahedral and similar to those of **1** and **2**.



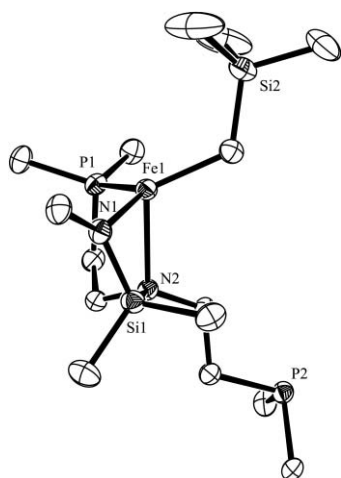
Scheme 1

Alkylation of **2** was also accomplished using LiCH₂SiMe₃, which afforded [N₂P₂]FeCH₂SiMe₃ (**5**) as colorless plate-like

Table 2 Selected bond lengths (Å) and angles (°) for $[\text{N}_2\text{P}_2]\text{FeCH}_2\text{SiMe}_3$ (**5**)

Fe(1)–N(1)	1.972(2)	Fe(1)–C(23)	2.066(3)
Fe(1)–N(2)	2.315(2)	Fe(1)–P(1)	2.4560(9)
N(1)–Fe(1)–C(23)	126.78(11)	N(1)–Fe(1)–N(2)	74.28(9)
C(23)–Fe(1)–N(2)	113.49(10)	N(1)–Fe(1)–P(1)	115.46(7)
C(23)–Fe(1)–P(1)	117.76(9)	N(2)–Fe(1)–P(1)	81.76(6)

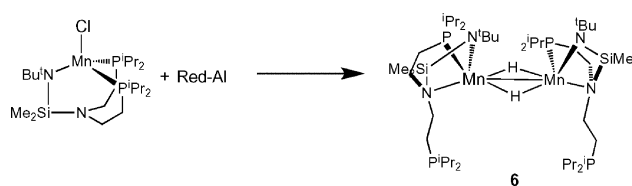
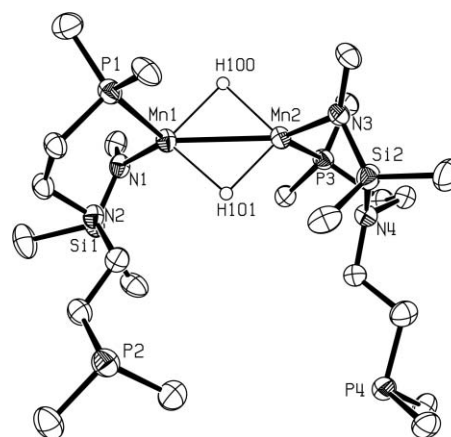
crystals in 77% yield following crystallization from pentane at -40°C . In the related Co system, the binding mode of the $[\text{N}_2\text{P}_2]$ ligand changed from $\kappa^4\text{-N}_2\text{P}_2$ to $\kappa^3\text{-N}_2\text{P}$ when the R group was changed from methyl to trimethylsilylmethyl.³⁰ An ORTEP diagram of **5** is displayed in Fig. 1 with selected bond lengths and angles provided in Table 2. Like the Co analogue, the Fe center lies in a mildly distorted tetrahedral geometry with angles of $126.78(11)^\circ$ {N(1)–Fe(1)–C(23)}, $113.49(10)^\circ$ {C(23)–Fe(1)–N(2)}, $115.46(7)^\circ$ {N(1)–Fe(1)–P(1)}, and $117.76(9)^\circ$ {C(23)–Fe(1)–P(1)}. The Fe(1)–C(23) bond distance of 2.066(3) Å is close to the corresponding parameters previously reported for the α -diimine Fe complex $[\text{ArN}=\text{C}(\text{CH}_3)\text{-C}(\text{CH}_3)=\text{NAr}]\text{Fe}(\text{CH}_2\text{SiMe}_3)_2$, Ar = 2,6-diisopropylphenyl, (2.042(3) and 2.072(3) Å)³⁷ and in the bis(imino)pyridine complex $(^i\text{PrPDI})\text{Fe}(\text{CH}_2\text{SiMe}_3)_2$ (2.062(3) and 2.054(3) Å).³⁸ The solution magnetic susceptibility was determined to be $5.1 \mu_{\text{B}}$, in agreement with a high-spin Fe(II) center. Unfortunately, efforts to generate the corresponding Mn alkyl complex were unsuccessful.

**Fig. 1** Thermal ellipsoid (50%) plot of **5**. Hydrogen atoms, *iso*-propyl methyl, and *tert*-butyl methyl groups have been omitted for clarity.

Attempts to isolate an $[\text{N}_2\text{P}_2]\text{Fe}$ hydride from **2** and reducing agents such as Red-Al[®], lithium aluminum hydride, and Super-Hydride[®] resulted in dark orange-brown solutions that did not yield any tractable material. Addition of trapping agents, such as PMe_3 , also did not lead to identifiable products. In contrast to **2**, complex **1** is a useful starting material for the bridging dihydride $\{([\text{N}_2\text{P}_2]\text{Mn})_2(\mu\text{-H})_2\}$ (**6**) (Scheme 2). Reaction of **1** with one equivalent of Red-Al[®] resulted in the isolation of colorless acicular crystals of **6** in 57% yield. The IR spectrum of **6** shows a weak, broad absorption at 1790 cm^{-1} , suggestive of a metal-hydride. The solid-state structure of **6** was determined *via* X-ray diffraction; the ORTEP diagram is shown in Fig. 2 with selected bond lengths

Table 3 Selected bond lengths (Å) and angles (°) for $\{([\text{N}_2\text{P}_2]\text{Mn})_2(\mu\text{-H})_2\}$ (**6**)

Mn(1)–N(1)	2.029(2)	Mn(1)–P(1)	2.5961(9)
Mn(1)–Mn(2)	2.7945(7)	Mn(1)–H(100)	2.07(2)
Mn(1)–H(101)	1.91(2)	Mn(2)–N(3)	2.032(3)
Mn(2)–P(3)	2.6244(9)	Mn(2)–H(101)	2.04(2)
Mn(2)–H(100)	2.04(2)		
N(1)–Mn(1)–P(1)	112.68(8)	N(1)–Mn(1)–Mn(2)	136.00(7)
P(1)–Mn(1)–Mn(2)	111.00(3)	N(1)–Mn(1)–H(100)	120.3(6)
P(1)–Mn(1)–H(100)	98.3(6)	Mn(2)–Mn(1)–H(100)	46.6(7)
N(1)–Mn(1)–H(101)	119.5(7)	P(1)–Mn(1)–H(101)	109.3(7)
Mn(2)–Mn(1)–H(101)	46.8(7)	H(100)–Mn(1)–H(101)	93.4(10)
N(3)–Mn(2)–P(3)	114.72(7)	N(3)–Mn(2)–Mn(1)	132.68(7)
P(3)–Mn(2)–Mn(1)	112.47(3)	N(3)–Mn(2)–H(100)	118.4(6)
P(3)–Mn(2)–H(100)	100.5(7)	Mn(1)–Mn(2)–H(100)	47.6(6)
N(3)–Mn(2)–H(101)	117.8(7)	P(3)–Mn(2)–H(101)	111.4(7)
Mn(1)–Mn(2)–H(101)	43.1(7)	H(100)–Mn(2)–H(101)	90.7(9)

**Scheme 2****Fig. 2** Thermal ellipsoid (50%) plot of **6**. Hydrogen atoms (with the exception of bridging hydrides), *iso*-propyl methyl, and *tert*-butyl methyl groups have been omitted for clarity.

and angles provided in Table 3. In contrast to $[\text{N}_2\text{P}_2]\text{CoH}$ which is monomeric with a $\kappa^4\text{-N}_2\text{P}_2$ bound ligand,³⁰ the Mn derivative **6** is dimeric and displays $\kappa^2\text{-NP}$ bound $[\text{N}_2\text{P}_2]$ ligands.³⁹ There is a short contact between the two Mn centers (2.7945(7) Å), which is less than typical Mn–Mn single bonds (ave. 2.842 Å) but is very close to a Mn=Mn double bond (ave. 2.791 Å).⁴⁰ The existence of a Mn–Mn interaction in **6** is further supported by magnetic susceptibility data (see below). The Mn–H bond distances of 1.91(2), 2.07(2), 2.04(2), and 2.04(2) Å are longer than those observed in the only other structurally characterized Mn dimer with two bridging hydrides $[\text{Mn}_2(\mu\text{-H})_2(\text{CO})_6(\mu\text{-dppm})]$ (1.59(5), 1.68(5), 1.76(5), and 1.81(5) Å), though little should be drawn from this observation as the distance between the Mn centers in $[\text{Mn}_2(\mu\text{-H})_2(\text{CO})_6(\mu\text{-dppm})]$ (2.699(2) Å) is significantly shorter than that observed in **6**.⁴¹

The solution magnetic susceptibility was found to be $3.4 \mu_B$ per Mn center, much lower than the theoretical value of $5.5 \mu_B$ ($S = 5/2$) for high-spin Mn(II). The difference between the observed and theoretical μ_{eff} values indicated an interaction between the two Mn centers might exist. To probe this interaction, SQUID data was collected on crystalline **6**. The μ_{eff} versus T plot shows a temperature dependence on the magnetic susceptibility consistent with direct communication between the two Mn centers even at 300 K (Fig. 3).⁴² The solution μ_{eff} may be larger than that observed in the solid-state due to the presence of a paramagnetic impurity resulting from the formation of monomer $[\text{N}_2\text{P}_2]\text{MnH}$ in solution.⁴³

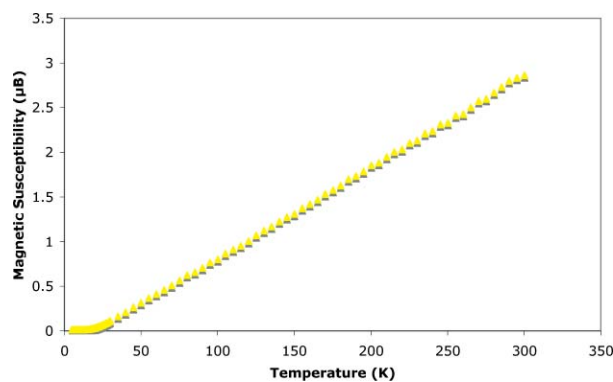


Fig. 3 SQUID data for **6**.

Reduction chemistry of **1** and **2**

Addition of sodium naphthalide to a suspension of **1** in THF at -40°C under an atmosphere of N_2 resulted in an immediate color change of colorless to dark red. Following the removal of solvent under vacuum, extraction with pentane, concentration, and cooling at -40°C , dark red crystals of $[\text{N}_2\text{P}_2]\text{Mn}(\mu\text{-N}_2)$ (**7**) were isolated in 24% yield. The solid-state structure of **7** was determined by X-ray crystallography. An ORTEP diagram is shown in Fig. 4 with selected bond lengths and angles provided in Table 4. As in **1**, each Mn center is four-coordinate in a tetrahedral environment, and the $[\text{N}_2\text{P}_2]$ ligand is bound $\kappa^3\text{-NP}_2$.²⁹ In **7**, however, the chloride ligand has been replaced by an end-on bridging N_2 moiety. Complex **7** represents only the second crystallographically characterized bridging dinitrogen manganese compound. The N–N bond length in **7** is 1.208(6) Å, significantly longer than the distance reported for $\{\eta^5\text{-C}_5\text{H}_4\text{CH}_3\text{Mn}(\text{CO})_2\}_2(\mu\text{-N}_2)$ ⁴⁴ (1.118(7) Å). The elongation of the N–N bond is likely due to

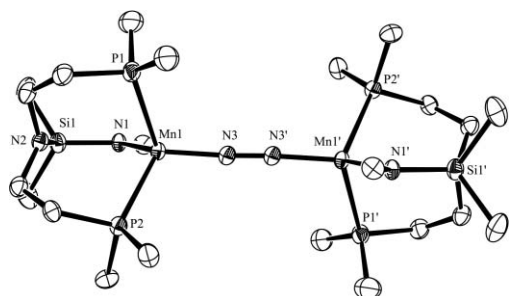


Fig. 4 Thermal ellipsoid (50%) plot of **7**. Hydrogen atoms, *iso*-propyl methyl, and *tert*-butyl methyl groups have been omitted for clarity.

Table 4 Selected bond lengths (Å) and angles ($^\circ$) for $[\text{N}_2\text{P}_2]\text{Mn}(\mu\text{-N}_2)$ (**7**)

Mn(1)–N(3)	1.860(3)	Mn(1)–N(1)	2.066(3)
Mn(1)–P(1)	2.5514(12)	Mn(1)–P(2)	2.5543(12)
N(3)–N(3')	1.208(6)		
N(3)–Mn(1)–N(1)	128.21(13)	N(3)–Mn(1)–P(1)	105.07(10)
N(1)–Mn(1)–P(1)	102.08(9)	N(3)–Mn(1)–P(2)	107.33(10)
N(1)–Mn(1)–P(2)	107.91(9)	P(1)–Mn(1)–P(2)	103.61(4)

increased π back-bonding into the π^* -orbital of the N_2 moiety as a result of the low coordination number observed in **7** and the lack of other π -accepting ligands such as CO. The Mn– N_2 bond distance (1.860(3) Å) is significantly shorter than that of the Mn(1)–N(1) amide bond (2.066(3) Å) but still longer than a typical Mn–N imido bond (ave. 1.651 Å).⁴⁰ The increased activation of the N–N bond seen in the X-ray structure of **7** is also reflected in the Raman spectrum where the $\nu_{\text{N-N}}$ is observed at 1685 cm^{-1} compared to 1975 cm^{-1} previously reported for $\{\eta^5\text{-C}_5\text{H}_4\text{CH}_3\text{Mn}(\text{CO})_2\}_2(\mu\text{-N}_2)$ (free N_2 : $\nu_{\text{N-N}} = 2329 \text{ cm}^{-1}$). The solution magnetic susceptibility was determined to be $8.7 \mu_B$, very close to the spin-only value of $8.9 \mu_B$ for two high-spin Mn(I) centers.

Reduction of the iron analogue **2** with KC_8 in THF at -40°C under an atmosphere of N_2 resulted in an immediate color change of yellow to dark red. Following removal of solvent under vacuum, a yellow-green solid was obtained. When redissolved in N_2 degassed pentane, the dark red color returned. Cooling of the red pentane solution at -40°C resulted in the isolation of $[\text{N}_2\text{P}_2]\text{Fe}_2(\mu\text{-N}_2)$ (**8**) as dark red crystals in 80% yield. The solid-state structure of **8**, determined *via* X-ray diffraction, is shown as an ORTEP diagram in Fig. 5 with selected bond lengths and angles provided in Table 5. As with **7**, compound **8** is a bridging dinitrogen complex possessing two tetrahedral metal centers bridged by a reduced, end-on N_2 moiety. The N–N bond distance in **8** is 1.166(3) Å and is less reduced than the N_2 in **7**. However, the N–N distance is still significantly longer than

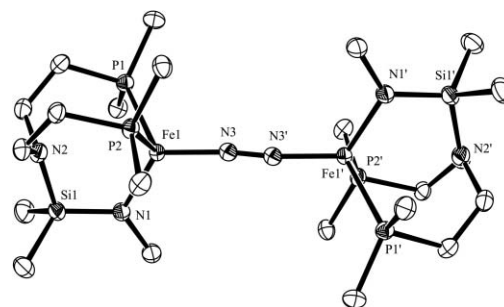


Fig. 5 Thermal ellipsoid (50%) plot of **8**. Hydrogen atoms, *iso*-propyl methyl, and *tert*-butyl methyl groups have been omitted for clarity.

Table 5 Selected bond lengths (Å) and angles ($^\circ$) for $[\text{N}_2\text{P}_2]\text{Fe}_2(\mu\text{-N}_2)$ (**8**)

Fe(1)–N(3)	1.8510(15)	Fe(1)–N(1)	1.9983(15)
Fe(1)–P(1)	2.4465(6)	Fe(1)–P(2)	2.3958(5)
N(3)–N(3')	1.166(3)		
N(3)–Fe(1)–N(1)	120.99(6)	N(3)–Fe(1)–P(1)	113.64(5)
N(1)–Fe(1)–P(1)	101.34(5)	N(3)–Fe(1)–P(2)	99.97(5)
N(1)–Fe(1)–P(2)	116.41(5)	P(1)–Fe(1)–P(2)	103.756(19)

the value observed in free N_2 (1.098 Å) and is similar to the related complexes $\{[\text{PhB}(\text{CH}_2\text{P}^i\text{Pr}_2)_3\text{Fe}\}\mu\text{-N}_2\}^{24}$ (1.138(6) Å) and $\{([\text{ArNC}(\text{tBu})_2\text{CH})\text{Fe}]_2\mu\text{-N}_2\}^{21}$ (1.182(5) Å), where Ar = 2,6-diisopropylaniline. Similar to **7**, the Fe– N_2 bond distance (1.8510(15) Å) is shorter than the Fe(1)–N(1) amide bond distance of 1.9983(15) Å and has some imido bond character (ave. 1.653 Å).⁴⁰ The Raman spectrum of **8** reveals a $\nu_{\text{N-N}}$ of 1760 cm^{-1} , similar to the corresponding value reported for $\{([\text{ArNC}(\text{tBu})_2\text{CH})\text{Fe}\}\mu\text{-N}_2\}^{21}$ (1778 cm^{-1}) and further supports the existence of a higher N–N bond order in **8** as compared to **7**. The solution magnetic susceptibility of **8** is 7.0 μ_B , slightly higher than the spin-only value of 6.9 μ_B for six unpaired electrons (two high-spin Fe(I) centers) but lower than the values seen in the related compounds $\{[\text{PhB}(\text{CH}_2\text{P}^i\text{Pr}_2)_3\text{Fe}\}\mu\text{-N}_2\}^{25}$ (8.2 μ_B) and $\{([\text{ArNC}(\text{tBu})_2\text{CH})\text{Fe}\}\mu\text{-N}_2\}^{22}$ (8.4 μ_B).

Though the structural features of **7** and **8** are similar, the binding strength of the N_2 moiety appears to differ significantly, even though only a small difference is seen in the N–N bond lengths. When a dark red solution of **7** is exposed to vacuum, no color change is observed. However, if the same experiment is performed on a solution of **8**, the solution changes color from red to lime green. This green color remains constant if the solution is held under vacuum or if an argon atmosphere is established. Once re-exposed to N_2 , the solution returns to dark red, reforming **8** as confirmed by its successful re-isolation.

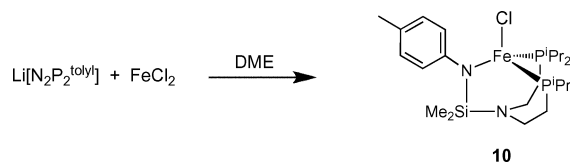
The green product may also be obtained by direct synthesis. Reduction of **2** with KC_8 under an argon atmosphere results in a color change of yellow to green. Following the removal of solvent under vacuum, extraction with Et_2O , concentration and cooling at -40°C , yellow-green crystals were obtained. Unfortunately, crystals suitable for an X-ray diffraction study have been elusive. The yield of this reaction has yet to be determined due to reformation of **8** upon exposure to N_2 .

Our initial assignment of the identity of this green complex, $[\text{N}_2\text{P}_2]\text{Fe}$ (**9**), is based on a number of experimental observations. Peters *et al.* recently reported an unstable Fe(I) complex that performed an intramolecular C–H bond activation to form an Fe(III) hydride species.⁴⁵ Though no structural data was reported, the IR spectrum of this complex revealed an Fe–H absorption at 2058 cm^{-1} . The solution IR spectrum of **9** lacks any features in the region typically associated with a M–H or an asymmetric N–N stretch (1600–2700 cm^{-1}), *i.e.* **9** does not appear to be an Fe(III) hydride or a monomeric Fe(I)– N_2 complex. It is also relevant to note that the Co(I) analogue, $[\text{N}_2\text{P}_2]\text{Co}$, is known and does not bind N_2 .³⁰

Ligand modification

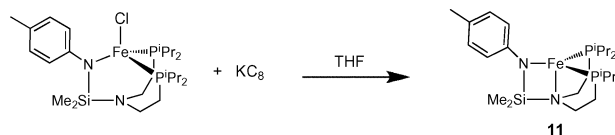
We recently reported the synthesis of the new ligand $[\text{N}_2\text{P}_2^{\text{tolyl}}]$, which was used to support Co(II) and Co(I) complexes.³⁰ Evaluation of the ν_{CO} and electrochemical data for Co complexes showed that $[\text{N}_2\text{P}_2]$ is a better donor than $[\text{N}_2\text{P}_2^{\text{tolyl}}]$, but the difference is minor. One aspect of the $[\text{N}_2\text{P}_2^{\text{tolyl}}]$ ligand that was not probed in the Co system was the difference in steric bulk on complex reactivity. Since the *p*-tolyl group penetrates farther away from the metal center than the *tert*-butyl group, we were curious about what effect this might have on the formation of bridging dinitrogen complexes.

Addition of $\text{Li}[\text{N}_2\text{P}_2^{\text{tolyl}}]$ to a suspension of FeCl_2 in DME resulted in an immediate color change of colorless to bright orange (Scheme 3). Following the removal of solvent under vacuum, extraction with THF, concentration, and cooling at -40°C , $[\text{N}_2\text{P}_2^{\text{tolyl}}]\text{FeCl}$ (**10**) was isolated as bright orange crystals in 70% yield; the solution magnetic susceptibility of this material is 4.7 μ_B . Given the similarities between the solid-state structures of $[\text{N}_2\text{P}_2]\text{CoI}$ and $[\text{N}_2\text{P}_2]\text{FeCl}$, it is reasonable to infer that the structure of **10** is similar to that of $[\text{N}_2\text{P}_2^{\text{tolyl}}]\text{CoI}$, which is tetrahedral and has similar metrical parameters to $[\text{N}_2\text{P}_2]\text{CoI}$.³⁰



Scheme 3

Reduction of **10** with KC_8 in THF under an atmosphere of N_2 resulted in a color change of bright orange to dark orange (Scheme 4). The resulting material, tentatively assigned $[\text{N}_2\text{P}_2^{\text{tolyl}}]\text{Fe}$ (**11**), shows good solubility in toluene and Et_2O . Though crystalline material has been obtained, the ideal crystallization conditions for obtaining X-ray quality crystals have yet to be determined. As gauged by both IR and Raman spectroscopy we found no evidence of N_2 coordination in isolated samples of **11**. Given the stability of **9** in the absence of N_2 , it is not unreasonable to believe that **11** has a similar structure to **9** (monomeric and N_2 free). The *p*-tolyl group could stabilize the lone pair of electrons on the amide nitrogen, rendering the Fe center less electron rich, and thus, perhaps, less amenable to N_2 binding. In addition, the lack of donation by the free pair of electrons on the amide nitrogen might encourage coordination of the basal nitrogen, which could also discourage N_2 coordination. Both $[\text{N}_2\text{P}_2]\text{Co}$ and $[\text{N}_2\text{P}_2^{\text{tolyl}}]\text{Co}$ have similar structural parameters and are monomeric,³⁰ and though **9** and **11** could be dimers, the formulations of these substances in the solid-state cannot be unambiguously established until X-ray quality crystals are obtained.



Scheme 4

Conclusions

This study has shown that the $[\text{N}_2\text{P}_2]$ motif is a competent supporting ligand for organometallic derivatives of Mn and Fe. In doing so, it adds further scope to the chemistry of this ligand system, which has now been shown to support a wide range of metal complexes from the main-group and both early and late metals in the d-transition series. While no Fe–H species could be observed, a dimeric bridging dihydride of Mn (**6**) was synthesized, and strong coupling between the two Mn(II) centers was found both in solution and the solid-state. The $[\text{N}_2\text{P}_2]$ ligand also stabilizes structurally similar Mn(I) (**7**) and Fe(I) (**8**) complexes possessing bridging dinitrogen moieties.

Notes and references

- 1 B. L. Small, M. Brookhart and A. M. A. Bennett, *J. Am. Chem. Soc.*, 1998, **120**, 4049–4050.
- 2 G. J. P. Britovsek, V. C. Gibson, B. S. Kimberley, P. J. Maddox, S. J. McTavish, G. A. Solan, A. J. P. White and D. J. Williams, *Chem. Commun.*, 1998, 849–850.
- 3 A. M. A. Bennett, *Chem.-Tech.*, 1999, **29**, 24–28.
- 4 B. L. Small and M. Brookhart, *J. Am. Chem. Soc.*, 1998, **120**, 7143–7144.
- 5 D. Reardon, G. Aharonian, S. Gambarotta and G. P. A. Yap, *Organometallics*, 2002, **21**, 786–788.
- 6 S. C. Bart, E. Lobkovsky and P. J. Chirik, *J. Am. Chem. Soc.*, 2004, **126**, 13794–13807.
- 7 A. R. Sadique, E. A. Gregory, W. W. Brennessel and P. L. Holland, *J. Am. Chem. Soc.*, 2007, **129**, 8112–8121.
- 8 E. A. MacLachlan and M. D. Fryzuk, *Organometallics*, 2006, **25**, 1530–1543.
- 9 M. Hirotsu, P. P. Fontaine, P. Y. Zavalij and L. R. Sita, *J. Am. Chem. Soc.*, 2007, **129**, 12690–12691.
- 10 M. D. Fryzuk, J. B. Love, S. J. Rettig and V. G. Young, *Science*, 1997, **275**, 1445–1447.
- 11 J. A. Pool, E. Lobkovsky and P. J. Chirik, *Nature*, 2004, **427**, 527–530.
- 12 C. E. Laplaza and C. C. Cummins, *Science*, 1995, **268**, 861–863.
- 13 D. V. Yandulov and R. R. Schrock, *Science*, 2003, **301**, 76–78.
- 14 J. R. Jennings, *Catalytic Ammonia Synthesis: Principles and Practice*, Plenum, New York, 1991.
- 15 B. E. Smith, *Science*, 2002, **297**, 1654–1655.
- 16 B. K. Burgess, *Chem. Rev.*, 1990, **90**, 1377–1406.
- 17 B. K. Burgess and D. J. Lowe, *Chem. Rev.*, 1996, **96**, 2983–3011.
- 18 J. B. Howard and D. C. Rees, *Chem. Rev.*, 1996, **96**, 2965–2982.
- 19 F. Barriere, *Coord. Chem. Rev.*, 2003, **236**, 71–89.
- 20 J. Scott, I. Vidyaratne, I. Korobkov, S. Gambarotta and P. H. M. Budzelaar, *Inorg. Chem.*, 2008, **47**, 896–911.
- 21 J. M. Smith, R. J. Lachicotte, K. A. Pittard, T. R. Cundari, G. Lukat-Rodgers, K. R. Rodgers and P. L. Holland, *J. Am. Chem. Soc.*, 2001, **123**, 9222–9223.
- 22 J. M. Smith, A. R. Sadique, T. R. Cundari, K. R. Rodgers, G. Lukat-Rodgers, R. J. Lachicotte, C. J. Flaschenriem, J. Vela and P. L. Holland, *J. Am. Chem. Soc.*, 2006, **128**, 756–769.
- 23 W. A. Chomitz and J. Arnold, *Chem. Commun.*, 2007, 4797–4799.
- 24 T. A. Betley and J. C. Peters, *J. Am. Chem. Soc.*, 2004, **126**, 6252–6254.
- 25 T. A. Betley and J. C. Peters, *J. Am. Chem. Soc.*, 2003, **125**, 10782–10783.
- 26 A. A. Danopoulos, J. A. Wright and W. B. Motherwell, *Chem. Commun.*, 2005, 784–786.
- 27 P. J. Alaimo, D. W. Peters, J. Arnold and R. G. Bergman, *J. Chem. Educ.*, 2001, **78**, 64–64.
- 28 C. Piguet, *J. Chem. Educ.*, 1997, **74**, 815–816.
- 29 W. A. Chomitz, S. F. Mickenberg and J. Arnold, *Inorg. Chem.*, 2008, **47**, 373–380.
- 30 (a) W. A. Chomitz and J. Arnold, submitted; (b) W. A. Chomitz and J. Arnold, *Chem. Commun.*, 2008, 3648–3650.
- 31 *SMART Area-Detector Software Package*, Bruker Analytical X-ray Systems, Inc., Madison, WI, 1995–99.
- 32 *SAINTE SAX Area-Detector Integration Program*, V7.06, Siemens Industrial Automation, Inc., Madison, WI, 2005.
- 33 *XPREP (v6.12) Part of the SHELXTL Crystal Structure Determination Package*, Bruker AXS Inc., Madison, WI, 1995.
- 34 *SADABS (v2.10) Siemens Area Detector ABSorption correction program*, George Sheldrick, 2005.
- 35 *XS Program for the Refinement of X-ray Crystal Structures, Part of the SHELXTL Crystal Structure Determination Package*, Bruker Analytical X-ray Systems Inc., Madison, WI, 1995–99.
- 36 *XL Program for the Refinement of X-ray Crystal Structures, Part of the SHELXTL Crystal Structure Determination Package*, Bruker Analytical Systems Inc., Madison, WI, 1995–99.
- 37 S. C. Bart, E. J. Hawrelak, A. K. Schmisser, E. Lobkovsky and P. J. Chirik, *Organometallics*, 2004, **23**, 237–246.
- 38 M. W. Bouwkamp, S. C. Bart, E. J. Hawrelak, R. J. Trovitch, E. Lobkovsky and P. J. Chirik, *Chem. Commun.*, 2005, 3406–3408.
- 39 S. G. Minasian and J. Arnold, *Dalton Trans.*, 2009, 106–110.
- 40 Cambridge Structural Database.
- 41 F. J. G. Alonso, M. G. Sanz, V. Riera, M. A. Ruiz, A. Tiripicchio and M. T. Camellini, *Angew. Chem. Int. Ed.*, 1988, **27**, 1167–1168.
- 42 J. F. Chai, H. P. Zhu, A. C. Stuckl, H. W. Roesky, J. Magull, A. Bencini, A. Caneschi and D. Gatteschi, *J. Am. Chem. Soc.*, 2005, **127**, 9201–9206.
- 43 C. C. Lu and J. C. Peters, *Inorg. Chem.*, 2006, **45**, 8597–8607.
- 44 K. Weidenhammer, W. A. Herrmann and M. L. Ziegler, *Z. Anorg. Allg. Chem.*, 1979, **457**, 183–188.
- 45 C. C. Lu, C. T. Saouma, M. W. Day and J. C. Peters, *J. Am. Chem. Soc.*, 2007, **129**, 4–5.